State Estimation and Control for Stochastic Quantum Dynamics with Homodyne Measurement

Stabilizing Qubits under Uncertainty

Binandeh Dehaghani, Nahid; Pedro Aguiar, A.; Wisniewski, Rafal

Published in:
IEEE Access

DOI (link to publication from Publisher):
10.1109/ACCESS.2024.3455170

Publication date:
2024

Document Version
Publisher's PDF, also known as Version of record

IEEE Access
Multidisciplinary ⋮ Rapid Review ⋮ Open Access Journal

Received 19 August 2024, accepted 2 September 2024, date of publication 5 September 2024,
date of current version 16 September 2024.

Digital Object Identifier 10.1109/ACCESS.2024.3455170

RESEARCH ARTICLE

State Estimation and Control for Stochastic Quantum Dynamics With Homodyne Measurement: Stabilizing Qubits Under Uncertainty

NAHID BINANDEH DEHAGHANI[1], (Graduate Student Member, IEEE),
A. PEDRO AGUIAR[1], (Senior Member, IEEE),
AND RAFAL WISNIEWSKI[2], (Senior Member, IEEE)
[1]SYSTEC-ARISE Research Center for Systems and Technologies, Faculty of Engineering, University of Porto, 4200-465 Porto, Portugal
[2]Department of Electronic Systems, Aalborg University, 9220 Aalborg, Denmark

Corresponding author: Nahid Binandeh Dehaghani (nahid@fe.up.pt)

This work was supported in part by the Foundation for Science and Technology (FCT) through National Funds (FCT/PIDDAC) within the PhD Grant 2021.07608.BD, the Associated Laboratory ARISE under Grant LA/P/0112/2020, the Research Center for Systems and Technology (SYSTEC) under Grants UIDB/00147/2020 and UIDP/00147/2020, and the project RELIABLE (DOI 10.54499/PTDC/EEI-AUT/3522/2020) under Grant PTDC/EEI-AUT/3522/2020.

ABSTRACT This paper introduces a Lyapunov-based control strategy alongside two filtering methods for controlling and estimating the evolution of coherence vector elements from sequential homodyne measurements. The methods include traditional quantum filtering and a novel extended Kalman filter, which explicitly addresses the dynamics of a stochastic master equation with correlated noise, thereby ensuring the quantum properties of the estimated state variable by design. We also explore scenarios where the system's Hamiltonian is unknown, demonstrating that both filters exhibit reduced performance with increased estimation errors. To address this, we propose a multiple model estimation scheme applicable to either filter. The estimated density operator is then controlled using the proposed switching-based Lyapunov scheme, which guarantees noise-to-state practical stability in probability. We demonstrate the effectiveness of our approach in stabilizing a qubit coupled to a leaky cavity under homodyne detection, even with uncertainty in the resonance frequency.

INDEX TERMS Quantum control, stochastic dynamics, quantum filtering, switching Lyapunov control.

I. INTRODUCTION

A particularly fertile domain within quantum control is feedback control, where the control strategy is dynamically adjusted based on real-time feedback signals emanating from the evolving system [1]. In this regard, significant advancements have been achieved in the development and enhancement of the underlying principles of quantum probability and filtering theory [2], [3], [4], [5], [6], [7].

The associate editor coordinating the review of this manuscript and approving it for publication was Xiaojie Su.

In this study, see Fig. 1, we spotlight a qubit undergoing continuous homodyne detection described by a stochastic master equation. Creating a controller is crucial because it customizes the control system to manage specific state transformation tasks based on the homodyne current measurements. Inherent stochasticity of the analyzed problem accentuates the complexity of the control task, as the controller must dynamically adapt to the random evolution of the quantum state in each trajectory. Additionally, discerning the actual state of the qubit solely from the instantaneous homodyne current proves challenging. Thus, a sophisticated

estimating mechanism is imperative to extract pertinent information about the qubit's state from the time series of measurement results. Herein, we outline our contributions.

- Using a state-space representation of a qubit's mixed state, we develop a framework for quantum state estimation via stochastic dynamics in Itô form. First, we implement traditional quantum filtering [4]. Then, we extend the Kalman filter to the quantum domain, handling nonlinearity and noise correlation while ensuring state estimates remain within the Bloch ball through a projection operator to maintain the physical relevance of estimated states. Finally, we develop a class of Multiple-Model Adaptive Estimators (MMAEs) to address uncertainties and fluctuations in the quantum system's Hamiltonian by running parallel filters and adjusting weights based on measurement data.
- We introduce a robust switching-based Lyapunov control strategy designed for quantum stochastic systems with state uncertainty. We show that our control scheme guarantees noise-to-state practical stability in probability, meaning the expected distance of the state from the target set is bounded by a monotone function of the variance of the estimation error over time.
- We consider a complete framework that combines quantum filtering with switching Lyapunov-based feedback control, ensuring robustness despite uncertainty and noise. It probabilistically guarantees practical convergence of the system's state to a small neighborhood of the desired invariant set, whose size degradates gracefully with the intensity of the estimation error.

It is worth noting that Lyapunov control approaches have been widely used in the field of quantum control for ensuring the stability of quantum systems or guiding them to a desired state [8], [9], [10]. More recently, a quantum measurement-based feedback control via switching strategies has been proposed in [11] for quantum systems that can be controlled with a series of driving dynamics. In addition, [12] analyzes switching techniques designed for the rapid stabilization of pure states and subspaces within quantum filtering equations. Our contribution lies in the design of a controller in a different setup of [11] and [12] with the aim of steering the system state ρ towards a pre-defined stationary target set, by directly using the estimate of ρ, and with noise-to-state practical stability guarantees.

Moreover, regarding Kalman-based filtering, several methodologies have been previously implemented in the quantum domain [7], [13]. Here, we go beyond the usual Kalman techniques, e.g., in [14], by explicitly addressing the fact that the quantum system exhibits correlated process noise with measurement noise. More importantly, we guarantee by design the properties of valid quantum states. As anticipated, we also show that the proposed Quantum Filter and Quantum Kalman Filter estimators, suffer from reduced performance under model uncertainties, leading to significant estimation errors. To mitigate this, we show that the proposed MMAE exhibits good performance and can be directly applied to any

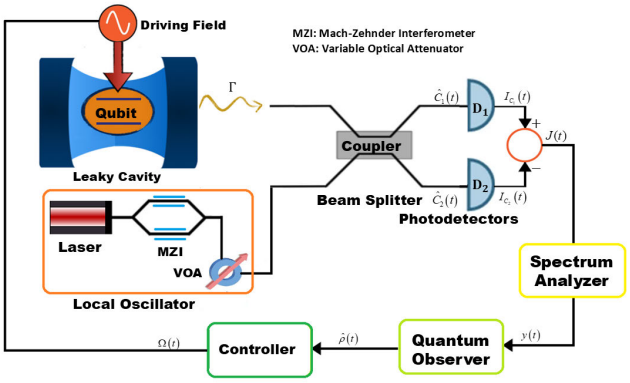

FIGURE 1. Illustration of the proposed configuration: A qubit coupled to a leaky cavity is continuously monitored via homodyne detection. The emitted radiation from the qubit is combined with a local oscillator laser at a beam splitter. The transformations of the field operators through the beam splitter are denoted by $C_1(t)$ and $C_2(t)$, which are then detected by photodetectors D_1 and D_2, respectively. The difference of the two produced signals I_{c1} and I_{c2} generates the resulting signal $J(t)$. This signal is sent to a quantum observer, which estimates the quantum state $\hat{\rho}(t)$. The estimated state is then transmitted to a controller. The controller adjusts the driving field $\Omega(t)$ through the control Hamiltonian to the qubit, aiming to generate and stabilize the qubit into a desired target set.

of the proposed estimators, demonstrating their applicability and effectiveness in different scenarios.

A. NOTATION

We use the superscripts T and $\dagger$ to denote the transpose and conjugate transpose of a matrix, respectively. Partial derivatives are denoted using ∂, where $\frac{\partial f}{\partial t}$ signifies the partial derivative with respect to the variable t. The notation $[\cdot,\cdot]$ represents a commutator of matrices. The imaginary unit is denoted by $i=\sqrt{-1}$, and the identity matrix is denoted by I. For a generic matrix A, the trace is shown by the operator $\mathrm{Tr}\{A\}$. The set of all quantum density operators ρ in a finite-dimensional complex Hilbert space $\mathbb{H}$ is denoted by $\mathbb{H}_\rho = \{\rho \in \mathscr{L}(\mathbb{H}) \mid \rho=\rho^\dagger,\ \rho\geq 0,\ \mathrm{Tr}(\rho)=1\}$, where $\mathscr{L}(\mathbb{H})$ denotes the set of linear operators on $\mathbb{H}$. For a variable X, the classical expectation value is indicated by $\mathbb{E}[X]$, while the quantum expectation value is denoted by $\langle X\rangle = \mathrm{Tr}\{X\rho\}$. The notation $U(2)$ represents the unitary group consisting of all 2×2 unitary matrices, which are relevant to qubit operations. We denote a continuous function $\zeta:\mathbb{R}_+\to\mathbb{R}_+$ to be of class $\mathscr{K}$ if it satisfies the following two properties: (i) Positive definiteness: $\zeta(s)>0$ for all $s\in\mathbb{R}_+\setminus\{0\}$, and $\zeta(0)=0$, and (ii) strict monotonicity: ζ is strictly increasing. We denote a continuous function $\eta:\mathbb{R}_+\times\mathbb{R}_+\to\mathbb{R}_+$ to be of class $\mathscr{KL}$ if it satisfies the following two properties: (i) For each fixed t, the function $\eta(\cdot,t)$ is of class $\mathscr{K}$, and (ii) For each fixed s, the function $\eta(s,\cdot)$ is decreasing and $\lim_{t\to\infty}\eta(s,t)=0$.

II. STOCHASTIC QUANTUM CONTROL AND ESTIMATION

Stochastic quantum dynamics encompass the complex interactions between quantum systems and classical

control mechanisms. This section delves into the mathematical frameworks and problem statements essential for controlling and estimating the states of such quantum systems.

A. QUANTUM STOCHASTIC EVOLUTION

The stochastic quantum dynamics can be accurately described by well-structured stochastic differential equations known as Stochastic Master Equations (SME). These equations define the relationships between the classical control input $\Omega(t)$, tuned by the controller, and the classical output $J(t)$ corresponding to instantaneous value of the observed measurements. For such a setup, as indicated in Fig. 1, the diffusive quantum stochastic master equation, interpreted in the context of Itô calculus, is expressed as [15]

$$\begin{aligned} d\rho(t) = &-i[H_d + \Omega(t)H_c, \rho(t)]dt + \Gamma\mathscr{D}[c_d]\rho(t)dt \\ &+ M\mathscr{D}[c_m]\rho(t)dt + \sqrt{\eta M}\mathscr{H}[c_m]\rho(t)dW(t), \end{aligned} \tag{1}$$

where the quantum density operator $\rho \in \mathbb{H}_\rho$. The unitary aspects of the dynamics (1) is characterized by the quantum mechanical system Hamiltonian composed of drift H_d and control H_c terms. The dissipative part of the dynamics is described through arbitrary Lindblad operators c_d and c_m, corresponding to decoherence and measurement channels. The superoperators $\mathscr{D}[c]\rho$ corresponding to dissipation, and $\mathscr{H}[c]\rho$ corresponding to measurement for a generic operator c are defined as follows

$$\begin{aligned} \mathscr{D}[c]\rho &= c\rho c^\dagger - \frac{1}{2}(c^\dagger c\rho + \rho c^\dagger c), \\ \mathscr{H}[c]\rho &= c\rho + \rho c^\dagger - \langle c + c^\dagger\rangle\rho. \end{aligned}$$

The coefficient $\Gamma > 0$ indicates the decay rate, $M > 0$ is the interaction strength corresponding to the measurement process, and $\eta \in [0,1]$ indicates the detector efficiency with $\eta = 1$ implying perfect detection and $\eta = 0$ lack of information about the quantum state. The differential $dW(t)$ denotes an infinitesimal Wiener increment satisfying Itô's lemma with $\mathbb{E}[dW(t)] = 0, \mathbb{E}[dW^2(t)] = dt$. The same Wiener process is shared by the outcome of classical measurement homodyne current

$$J(t) = \sqrt{\eta M}\langle c_m + c_m^\dagger\rangle + \xi(t), \tag{2}$$

where $\xi(t) = dW(t)/dt$, follows Gaussian white noise properties with $\mathbb{E}[\xi(t)\xi(t')] = \delta(t-t')$.

B. PROBLEM STATEMENT

This subsection outlines the primary two research objectives pursued in this paper.

Problem 1: Given the quantum system presented in (1)-(2), develop a set of estimators to directly estimate the evolution of the density operator $\rho(t)$ from the continuous sequence of homodyne current measurements. In addition, consider that the drift Hamiltonian H_d contains unknown constant parameters.

Prior to expressing the second problem, we introduce the following stability definition pertinent to the stochastic quantum system problem at hand, drawing upon the frameworks in [16] and [17].

Definition 1: (Noise-to-State Practically Stable in Probability): Let χ be a closed and invariant set under the dynamics governed by the stochastic differential equation in Itô form

$$d\rho(t) = f(\rho)dt + g(\rho)\sigma(t)dW(t),$$

where $\rho \in \mathbb{H}_\rho$, $\sigma(t)$ is the intensity of noise at time t, and $W(t)$ denotes a 1-dimensional standard Wiener process. The set χ is noise-to-state practically stable (NSpS) in probability if, for every $\varepsilon > 0$, there exists a function $\beta \in \mathscr{KL}$, a function $\gamma \in \mathscr{K}$, and a non-negative real number $b \geq 0$, ensuring that for every initial density operator $\rho(0) \in \mathbb{H}_\rho$, the following holds with probability at least $1-\varepsilon$, for every $t \geq 0$

$$\mathbb{P}\left\{d(\rho(t),\chi) < \beta(d(\rho(0),\chi),t) + \gamma(\sup_{\tau\in[0,t]}\sigma^2(\tau)) + b\right\} \geq 1-\varepsilon \tag{3}$$

If $b = 0$, χ is noise-to-state stable (NSS) in probability.

Remark 1: Note that NSpS implies that the set χ is asymptotically practically stable in probability, that is, condition (3) holds without the term $\gamma(\sup_{\tau\in[0,t]}\sigma^2(\tau))$, (but maybe with a different b) since $\sigma(t)$ is bounded. Moreover, in that case, if $\beta(r,t) = cre^{-\lambda t}$ for some $c > 0$ and $\lambda > 0$, the set χ is said to be practically exponentially stable in probability.

Definition 1 is introduced to measure the resilience of a quantum system's stability in the face of noise. It ensures that, probabilistically, the system's state stays within a practical vicinity of the invariant set χ, notwithstanding the influence of quantum noise. The extent of this vicinity is contingent upon the intensity of the noise, as characterized by the variance of the Wiener process $W(t)$.

We can now proceed with the second problem. To this end, let χ_f be a desired target state characterized by all the elements $\rho_f \in \mathbb{H}_\rho$ that commutes with the drift Hamiltonian H_d, that is, $[\rho_f, H_d] = 0$. This commutation condition ensures that the target states ρ_f remain invariant under the evolution governed by H_d. Then, the goal is the following.

Problem 2: Using the solutions to Problem 1 to estimate the system's state $\rho(t)$, design a controller that commands the signal $\Omega(t)$ with the aim of steering $\rho(t)$ from an arbitrary initial state $\rho_0 \in \mathbb{H}_\rho$, towards a stationary point within the predetermined target set χ_f. Moreover, the controller should guarantee that χ_f is NSpS with respect to the estimation error variance.

III. ESTIMATION TECHNIQUES IN STOCHASTIC QUANTUM DYNAMICS

This section introduces and elaborates on three estimation techniques: Quantum Filter Estimator, Quantum Extended Kalman Filter Estimator, and finally a Multiple-Model Adaptive Estimator to address the uncertainty on the drift

Hamiltonian H_d. In the following, we leverage the fact that a general mixed state of a qubit can be expressed as a linear combination of the Pauli matrices, which, along with the identity matrix, form a basis for the 2×2 self-adjoint matrices, i.e.,

$$\rho(t) = \frac{1}{2}I + \frac{1}{2}\sum_{k=1}^{3} x_k(t)\sigma_k, \tag{4}$$

where the real-valued functions $x_k(t) = \langle \sigma_k \rangle$ are the coordinates of a point within the unit ball and are taken to be components of the so-called coherence vector $\mathbf{x}(t) = [x_1(t), x_2(t), x_3(t)]^T \in \mathbb{R}^3$. By rewriting (1) one attains the following stochastic system dynamics for $\mathbf{x}(t)$ in Itô form

$$d\mathbf{x}(t) = \mathbf{f}(\mathbf{x}, \Omega(t))dt \ + \mathbf{g}(\mathbf{x})dW(t), \tag{5}$$

where $\mathbf{f}(\mathbf{x}, \Omega) = [f_1(\mathbf{x}, \Omega), f_2(\mathbf{x}, \Omega), f_3(\mathbf{x}, \Omega)]^T$ and $\mathbf{g}(\mathbf{x}) = [g_1(\mathbf{x}), g_2(\mathbf{x}), g_3(\mathbf{x})]^T$, whose elements for $k = 1, 2, 3$ are

$$\begin{aligned}\mathbf{f}_k(\mathbf{x}, \Omega) &= -i\,\mathrm{Tr}\{[H_d + \Omega(t)H_c, \rho(t)]\sigma_k\} \\ &\quad + \mathrm{Tr}\{(\Gamma\mathscr{D}[c_d] + M\mathscr{D}[c_m])\,\rho(t)\sigma_k\}, \\ \mathbf{g}_k(\mathbf{x}) &= \sqrt{\eta M}\,\mathrm{Tr}\{\mathscr{H}[c_m]\rho(t)\sigma_k\},\end{aligned}$$

with $\rho(t)$ substituted by (4). Accordingly, by rewriting the output equation (2), one attains

$$dy(t) = h(\mathbf{x}(t))dt + dV(t), \tag{6}$$

where the term $dV(t) = dW(t) + dZ(t)$ includes an additional infinitesimal Wiener increment with $\mathbb{E}[dZ(t)] = 0$, $\mathbb{E}[dZ^2(t)] = \sigma_z^2 dt$ corresponding to the measurement noise associated with the spectrum analyzer, and the term $h(\mathbf{x}(t))$ is given as

$$h(\mathbf{x}) = \frac{\sqrt{\eta M}}{2}\left(\mathrm{Tr}\{c_m + c_m^\dagger\} + \sum_{k=1}^{3} x_k(t)\,\mathrm{Tr}\{(c_m + c_m^\dagger)\sigma_k\}\right).$$

A. QUANTUM FILTER ESTIMATOR

The Quantum Filter Estimator is a fundamental tool in the estimation of quantum states. It provides a systematic approach to updating the state of a quantum system based on continuous measurement results. This estimator relies on the principles of quantum measurement theory and stochastic calculus to produce an estimate of the quantum state in real-time. In particular, since the quantum stochastic dynamics (1) is inherently a filtering equation, one can use it to predict the estimated state $\hat{\mathbf{x}}_{QF}(t)$ following the approach in [4], but in our case adapted for the coherence vector dynamics in (5), which results in

$$d\hat{\mathbf{x}}_{QF}(t) = \mathbf{f}(\hat{\mathbf{x}}_{QF}(t), \Omega(t))\,dt \ + \mathbf{g}(\hat{\mathbf{x}}_{QF}(t))(dy(t) - h(\hat{\mathbf{x}}_{QF})dt). \tag{7}$$

Here, $\hat{\mathbf{x}}_{QF}(t)$ represents the estimated state vector of quantum filtering equation at time t, $\mathbf{f}(t, \hat{\mathbf{x}}_{QF}(t))$ is the drift term, and $\mathbf{g}(\hat{\mathbf{x}}_{QF}(t))$ is the diffusion term influenced by the Wiener increment $dW(t)$, that in (7) is replaced by the innovation term $dy(t) - h(\hat{\mathbf{x}}_{QF})dt$.

B. QUANTUM KALMAN FILTER ESTIMATOR

The Quantum Kalman Filter Estimator extends the classical Kalman filter to the quantum domain. It is particularly useful for systems where the noise and disturbances can be modeled as Gaussian processes. By leveraging the properties of the Kalman filter, this estimator offers a robust and efficient means of tracking the evolution of quantum states under noisy conditions, yielding high-quality estimates in the presence of measurement and process noise while also providing the associated confidence or uncertainty levels. It is however important to stress that in this setup one have first to deal with the following points: (i) the stochastic system dynamics for the coherence vector in (5) is nonlinear; (ii) the noise in the output equation (6) is correlated with process noise in (5) by noting that dV includes dW; and (iii) the coherence vector space for a qubit is a ball with radius 1, known as the Bloch ball, thereby satisfying $\|\mathbf{x}\|^2 \leq 1$. To address (i), we apply an Extended Kalman Filter (EKF) based approach by linearizing the non-linear functions around the current estimate using a first-order Taylor expansion. For (ii), we make use of a de-correlating approach, see [18], but tailored for our case, such that the new transformed equivalent system satisfies the property of uncorrelated process and measurement noises, and therefore one can then make use of the standard EKF equations. To address (iii), we integrate the structural properties of a valid quantum state into the observer equations by constraining the state estimate $\hat{\mathbf{x}}_{KF}(t)$ at the update equation to always belong to the Bloch ball. To this end, we define the following operator acting on the coherence vector $\mathbf{x}$ and a real vector $\mathbf{a} \in \mathbb{R}^3$ as

$$\mathbf{x} \oplus \mathbf{a} = \mathrm{Proj}\,(\mathbf{x} + \mathbf{a}), \tag{8}$$

where the operator $\mathrm{Proj}(\mathbf{x}) = 1/\max\{1, \|\mathbf{x}\|\}\mathbf{x}$ projects $\mathbf{x}$ onto the closed ball. The operator (8) is pivotal within our proposed filtering algorithm, ensuring that the state and consequently the estimate of the density matrix adheres to the necessary properties of a density operator, and maintains the physical relevance of our estimated states.

With the established setup, we proceed to construct a quantum Kalman filter estimator. In this framework, we treat the measurement noise $dW(t)$ and the noise of spectrum analyzer $dZ(t)$ uncorrelated, that is $\mathbb{E}[dW(t)dZ(t)] = 0$. Then, its correlation with process noise is given by $\mathbb{E}[dW(t)dV(t)] = dt$ since we have been considered $\mathbb{E}[dW^2(t)] = dt$. Note also that the variance $\mathbb{E}[dV^2(t)]$ is defined as $\mathbb{E}[dV^2(t)] = \sigma_v^2 dt$, with $\sigma_v^2 = (1 + \sigma_z^2)$. Now, we establish the following result.

Proposition 1: Consider the stochastic differential equation (SDE)

$$d\bar{\mathbf{x}} = \bar{\mathbf{f}}(\bar{\mathbf{x}}, \Omega, dy)dt + \mathbf{g}(\bar{\mathbf{x}})d\bar{W}(t), \tag{9}$$

where

$$\bar{\mathbf{f}}(\bar{\mathbf{x}}, \Omega, dy)dt = \mathbf{f}(\bar{\mathbf{x}}, \Omega)dt - \bar{\sigma}\,\mathbf{g}(\bar{\mathbf{x}})h(\bar{\mathbf{x}})dt + \bar{\sigma}\,\mathbf{g}(\bar{\mathbf{x}})dy,$$

$\bar{\sigma} = 1/(1 + \sigma_z^2)$, and $d\bar{W} = dW - \bar{\sigma}\,dV$. Then, the process and measurement noises associated with the system formed by (9)

and (6) are uncorrelated, that is, $\mathbb{E}[d\bar{W}dV] = 0$. *Moreover, (9) is equivalent to (5) in the sense that if both SDEs start with the same initial condition and all the exogenous signals have the same trajectory, then* $\mathbf{x}(t) = \bar{\mathbf{x}}(t)$, *for every* $t \geq t_0$.

Proof: To show uncorrelated noises, we compute

$$\mathbb{E}[d\bar{W}(t)dV(t)] = \mathbb{E}[dW(t)dV(t)] - \bar{\sigma}\mathbb{E}[dV^2(t)] = 0.$$

To show the equivalence of both SDEs, we first start to note using (6) that the term $\bar{\sigma}\mathbf{g}(\mathbf{x})\big(dy - h(\mathbf{x})dt - dV\big)$ is zero. If we now add this null term to the right-hand-side of (5), and replace the variable $\mathbf{x}$ by $\bar{\mathbf{x}}$, we obtain precisely (9). □

We can now propose our state estimator that continuously updates its state estimate $\hat{\mathbf{x}}_{KF}(t)$ as new measurements are acquired through the propagation and update steps for the state and covariance matrix. In the propagation step, the current estimate of the state is propagated through the deterministic system dynamics

$$d\hat{\mathbf{x}}_{KF}^{-}(t) = \bar{\mathbf{f}}\hat{\mathbf{x}}_{KF}(t), \Omega(t), y(t))\, dt, \tag{10}$$

producing an a priori state estimate $\hat{\mathbf{x}}_{KF}^{-}(t)$. Similarly, an a priori estimation of the prediction error covariance matrix $P_{3\times 3}$ is computed as

$$dP^{-}(t) = (A(t)P(t) + P(t)A^{\dagger}(t) + G(t)\sigma_{\bar{w}}^{2}(t)G^{\dagger}(t))dt \tag{11}$$

for which the initial guess $P(0) = P_0$ encodes the confidence in the estimate of the initial condition $\hat{\mathbf{x}}_{KF}(0)$, and $\sigma_{\bar{w}}^{2} = 1 + \bar{\sigma}$.

Note that in (11), to evaluate the propagation of P, we need to compute the matrices $A(t) = \frac{\partial \bar{\mathbf{f}}(\mathbf{x},\Omega)}{\partial \mathbf{x}}$ and $G(t) = \frac{\partial \mathbf{g}(\mathbf{x})}{\partial \mathbf{x}}$. It turns out that only the term $\mathbf{g}(\mathbf{x})$ introduces a nonlinear term (in fact quadratic) in $\mathbf{x}$. All the other ones are linear with $\mathbf{x}$, and therefore the linearizations for these terms are not approximations. This is not surprising since the Lindblad equation can be transformed into an inhomogeneous linear vector equation using the coherence vector formulation [19].

Next, the update step integrates the most recent measurement by updating the prediction equations (10) and (11) to obtain the a posteriori estimates

$$\hat{\mathbf{x}}_{KF}(t) = \hat{\mathbf{x}}_{KF}^{-}(t) \oplus K(t)\,(dy(t) - h(\mathbf{x}(t))dt)\,,$$
$$P(t) = P^{-}(t) - P^{-}(t)C^{\dagger}\sigma_{v}^{-2}CP^{-}(t).$$

Here, the Kalman gain is computed as $K(t) = P(t)C^{\dagger}\sigma_{v}^{-2}$, where $C = \big[c_1, c_2, c_3\big]$, with $c_k = \frac{\sqrt{\eta M}}{2}\mathrm{Tr}\Big\{(c_m + c_m^{\dagger})\sigma_k\Big\}$, $k = 1, 2, 3$. By estimating the components of the Bloch vector, we can then reconstruct an estimate for the density matrix as follows:

$$\hat{\rho}(t) = \frac{1}{2}I + \frac{1}{2}\sum_{k=1}^{3}\hat{x}_{kKF}(t)\sigma_k. \tag{12}$$

We can now state the following result.

Proposition 2: Consider the proposed extended Kalman-based filter with initial condition $\hat{\rho}_0 \in \mathbb{H}_\rho$, *which implies an adequate initial condition* $\hat{\mathbf{x}}_{KF}(0)$. *Then, the state estimate* $\hat{\rho}(t)$ *leaves in* $\mathbb{H}_\rho$ *for every* $t \geq 0$.

Proof: In the propagation step, the coherence vector $\hat{\mathbf{x}}_{KF}(t)$ is the solution of the differential equation (10), which from Proposition 1 is equivalent to the deterministic part of (5). In the measurement step, we make use of the operator (8), which guarantees that $\|\hat{\mathbf{x}}_{KF}(t)\|^2 \leq 1$, which in turn implies positive semi-definiteness of $\hat{\rho}(t)$, and norm preservation since $\mathrm{Tr}\big\{\frac{I}{2} + \sum_k \hat{\mathbf{x}}_{kKF}(t)\sigma_k\big\} = 1$ using the fact that $\mathrm{Tr}(\sigma_k) = 0$. □

C. MULTIPLE-MODEL ADAPTIVE ESTIMATOR

This section presents a class of Multiple Model Adaptive Estimators (MMAEs) designed to address the challenges of quantum systems with parametric model varying dynamics or uncertainties, more precisely, in the quantum-mechanical Hamiltonian. The MMAE operates with a finite number N of selected models from the original (potentially infinite) set of system models and consists of two main components: i) a dynamic generator for N weighting signals $p_\ell(t)$, $\ell = 1, \ldots, N$, and ii) a bank of N estimators, each designed based on one of the selected models. In our case, the estimators are precisely either the Quantum estimator or the Extended Kalman filter presented in previous subsections designed to a specific value of H_d. The state estimate is produced by a weighted sum of the local state estimates $\hat{\mathbf{x}}_\ell(t)$, i.e.,

$$\hat{\mathbf{x}}(t) = \sum_{\ell=1}^{N} p_\ell(t)\hat{\mathbf{x}}_\ell(t).$$

By employing a set of parallel filters, each corresponding to a different model of the system's dynamics, the MMAE adapts to the most likely model based on measurement data. This provides a flexible and accurate estimation method capable of handling sudden changes in the system's behavior or parameters.

The evolution of each dynamic weight $p_\ell(t)$ is set to be piecewise constant, updating its value at instants of time $t = t_k$, according to following equation, [20]:

$$p_\ell(t_{i+1}) = \frac{\beta_\ell e^{-w_\ell(t_k)}}{\sum_{j=1}^{N} p_j(t_k)\beta_j e^{-w_j(t_k)}} p_\ell(t_k), \tag{13}$$

In (13), β_ℓ is a positive weighting constant value and $w_\ell(t_k)$ is a scalar continuous function called an error measuring function that maps the measurable signals of the quantum system and the states of the ℓ^{th} local estimator to a nonnegative real value. This error measuring function evaluates the discrepancy between the observed measurements and the predicted state from the ℓ^{th} model. An example is $w_\ell(t_k) = \|y_\ell(t_k) - h(\mathbf{x}_\ell(t_k)\|^2$. It can be proved (using similar arguments as in [20]) that due to the particular structure of equation (13), the weights $p_\ell(t)$ are positive, bounded, and the overall sum $\sum_{\ell=1}^{N} p_\ell(t)$ is always one for all $t \geq 0$, independently of the error measuring function $w_\ell(t)$. In this paper, we implemented the MMAE method for both Quantum Filter (QF) and Quantum Extended Kalman Filter (KF). The obtained results are presented in Section V.

IV. LYAPUNOV-BASED STATE FEEDBACK CONTROL

This section addresses Problem 2. Drawing inspiration from the concepts presented in [21], we begin by considering a state $\rho_f \in \chi_f$, and select a matrix $\Pi = I - \rho_f$. This selection leads us to define the Lyapunov function as

$$V(\rho) = \mathrm{Tr}\{\Pi\rho\}. \tag{14}$$

It is important to note that Π is Hermitian, ensuring that it possesses real eigenvalues. Furthermore, Π is positive semi-definite, which guarantees that the Lyapunov function $V(\rho)$ is non-negative for all states ρ, i.e., $V(\rho(t)) \geq 0$. Additionally, a significant characteristic of Π is its commutativity with the final state ρ_f, that is, $[\rho_f, \Pi] = 0$.

Remark 2: Stationary points of the Lyapunov function $V(\rho)$ are identified as states $\bar{\rho}$ that commute with ρ_f, see [21], i.e., $[\bar{\rho}, \rho_f] = 0$. Given the definition of $\Pi = I - \rho_f$, this commutation property implies $[\bar{\rho}, \Pi] = 0$.

We initially derive a controller to minimize $V(\rho)$, assuming access to the actual state $\rho(t)$.

Theorem 1: Consider the quantum system (1) and let $\chi_f = \{\rho \in \mathbb{H} : [\rho, \Pi] = 0\}$ be the desired stationary set. Consider the feedback control law

$$\Omega(t) = \begin{cases} -i\dfrac{\Upsilon_0}{\Upsilon_1}, & \text{for } t \in [t_{k-1}, t_k),\ k = 1, 3, 5, \ldots \\ 0, & \text{otherwise} \end{cases} \tag{15}$$

where $\Upsilon_0 = \Gamma\,\mathrm{Tr}\{\Pi\mathscr{D}[c_d]\rho\} + M\,\mathrm{Tr}\{\Pi\mathscr{D}[c_m]\rho\} + \alpha\,\mathrm{Tr}\{\Pi\rho\}$, with $\alpha \in \mathbb{R}^+$, and $\Upsilon_1 = \mathrm{Tr}\{\Pi[H_c, \rho]\}$. In the above, we set the control value to switch at event times $\{t_0, t_1, \ldots\}$ when Υ_1 crosses an $\varepsilon > 0$ value and the period of time between the last switching and current is larger than some dwell time, that is, t_k is defined as

$$\begin{cases} t_k = \min\limits_t\{t \geq t_{k-1} + \Delta_1 : \Upsilon_1 \leq \varepsilon\} & \text{for } k \text{ odd}, \\ t_k = \min\limits_t\{t \geq t_{k-1} + \Delta_2 : \Upsilon_1 \geq \varepsilon\} & \text{for } k \text{ even}, \end{cases}$$

for some appropriate dwell times $\Delta_1, \Delta_2 \in \mathbb{R}^+$. Then, the resulting closed-loop system exhibits the property that the set χ_f is practically exponentially stable in probability.

Proof: Given that ρ_f is selected to commute with Π, it follows that ρ_f becomes a stationary point of the Lyapunov function $V(\rho)$, as discussed in [21]. Furthermore, according to Remark 2, the set χ_f is identified as a stationary set. To investigate its stability, we consider the infinitesimal generator of $\rho(t)$ applied to $V(\rho)$. This analysis involves the diffusion process described in (1) and leverages the Itô formula, resulting in

$$\begin{aligned} L(V(\rho)) = \mathrm{Tr}\big\{\Pi^T\big(&-i[H_d, \rho(t)] + \Gamma\mathscr{D}[c_d]\rho(t) \\ &+ M\mathscr{D}[c_m]\rho(t) - i[H_c, \rho(t)]\Omega(t)\big)\big\} \\ &+ \frac{1}{2}\mathrm{Tr}\big\{Z(\rho)H_V Z^T(\rho)\big\} \end{aligned}$$

where $L(V(\rho))$ is the quantum Markov generator for the Lyapunov function V, and $Z(\rho) = \sqrt{\eta M}\,\mathscr{H}[c_m]\rho(t)$. Note that the last term is zero because the Hessian matrix H_V of $V(\rho)$ is null. Considering the commutation relation $[\rho_f, H_d] = 0$ and the definition $\Pi = I - \rho_f$, we deduce $[\Pi, H_d] = 0$ since $[I - \rho_f, H_d] = -[\rho_f, H_d] = 0$. By employing the trace property $\mathrm{Tr}\{A[B, C]\} = \mathrm{Tr}\{C[A, B]\}$, it follows that $\mathrm{Tr}\{\Pi[H_d, \rho]\} = \mathrm{Tr}\{\rho[\Pi, H_d]\} = 0$. Thus, we obtain

$$\begin{aligned} L(V(\rho)) = &-i\Omega(t)\,\mathrm{Tr}(\Pi[H_c, \rho(t)]) + \Gamma\,\mathrm{Tr}(\Pi\mathscr{D}[c_d]\rho(t)) \\ &+ M\,\mathrm{Tr}(\Pi\mathscr{D}[c_m]\rho(t)). \end{aligned} \tag{16}$$

At this point, our objective is to identify a control function $\Omega(t)$ that satisfies $L(V(\rho)) \leq -\alpha V(\rho)$, ensuring that $V(t) = V(\rho(t))$ is a supermartingale and decreases exponentially with a rate $\alpha > 0$. Among the potential solutions, we opt for the one that minimizes the control effort $\Omega^2(t)$ pointwise in time. Hence, we seek $\Omega(t)$ that solves the optimization problem:

$$\begin{aligned} &\underset{\Omega(t)}{\text{minimize}}\ \Omega^2(t) \\ &\text{subject to}\ -i\Omega(t)\Upsilon_1 + \Upsilon_0 \leq 0. \end{aligned}$$

The solution to this optimization problem is precisely the control law presented in (15). Caution is advised when Υ_1 approaches zero to prevent computational inaccuracies and excessive control signal magnitudes. As a preventive measure, the control strategy switches $\Omega(t)$ to zero once $\Upsilon_1 \leq \varepsilon$. To avoid Zeno behavior, characterized by an infinite number of switches within a finite time, we enforce a minimum dwell time between switching, $t_k - t_{k-1} > \Delta$.

Taking now into account the results and reasoning presented in [22] for switching systems with stable and unstable modes, and acknowledging that $L(V)$ remains bounded when $\Omega = 0$, the practical stability in probability of the set χ is conclusively established by noticing that $L(V) \leq -\eta(V) + \eta_0$, for some class $\mathscr{K}$ function η and constant $\eta_0 \geq 0$. □

We now adapt the proposed controller for the case that we do not have direct access to the state $\rho(t)$. By applying the methodology from the previous section, we compute an estimated state $\hat{\rho}(t)$ and use it in place of $\rho(t)$. The next result shows that we still recover practically stability in probability and moreover that the set χ_f is NSpS with respect to the estimation error.

Theorem 2: Consider the same conditions of Theorem 1, but now replacing (15) by

$$\Omega(t) = \begin{cases} -i\dfrac{\hat{\Upsilon}_0}{\hat{\Upsilon}_1}, & \text{for } t \in [t_{k-1}, t_k),\ k = 1, 3, 5, \ldots \\ 0, & \text{otherwise} \end{cases} \tag{17}$$

where $\hat{\Upsilon}_0 = \Gamma\,\mathrm{Tr}\{\Pi\mathscr{D}[c_d]\hat{\rho}\} + M\,\mathrm{Tr}\{\Pi\mathscr{D}[c_m]\hat{\rho}\} + \alpha\,\mathrm{Tr}\{\Pi\hat{\rho}\}$, with $\alpha \in \mathbb{R}^+$, and $\hat{\Upsilon}_1 = \mathrm{Tr}\{\Pi[H_c, \hat{\rho}]\}$ with $\hat{\rho}$ denoting the output estimate of the quantum observer. Let $\tilde{\sigma}^2(t)$ be the incremental variance associated to the noisy estimation error $\mathrm{Tr}\{\tilde{\rho}\} = \mathrm{Tr}\{\rho - \hat{\rho}\}$, which is considered to be bounded. Then, the set χ_f is NSpS with respect to $\tilde{\sigma}^2(t)$.

Proof: From (16), it follows that $L(V(\rho))$ satisfies

$$L(V(\rho)) = -i\hat{\Upsilon}_1\Omega(t) + \hat{\Upsilon}_0 - i\tilde{\Upsilon}_1\Omega(t) + \tilde{\Upsilon}_0, \tag{18}$$

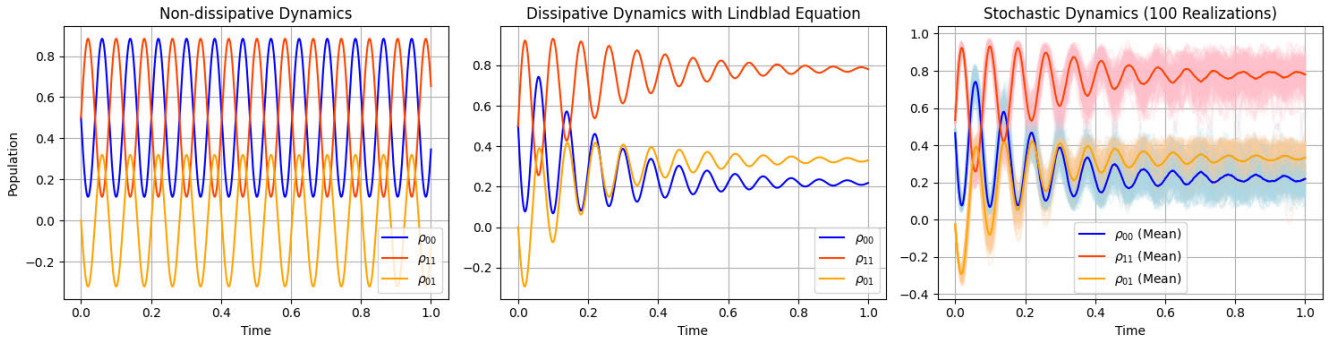

FIGURE 2. **Comparative evolution of quantum state populations. This figure illustrates the population dynamics of a quantum system under three different scenarios: (a) Non-dissipative dynamics, (b) Dissipative dynamics with the Lindblad equation, and (c) Stochastic dynamics over 100 realizations. In each subplot, the populations $\rho_{00}(t)$, $\rho_{11}(t)$, and the real part of the off-diagonal $\rho_{01}(t)$ (or $\rho_{10}(t)$) are plotted in time. The non-dissipative dynamics exhibit periodic oscillations, the dissipative dynamics show damped oscillations leading to steady-state populations, and the stochastic dynamics reveal ensemble-averaged behaviors with individual realizations contributing to the shaded regions.**

where $\tilde{\Upsilon}_0 = \Upsilon_0 - \hat{\Upsilon}_0$ and $\tilde{\Upsilon}_1 = \Upsilon_1 - \hat{\Upsilon}_1$. Using Proposition 2, we deduce that $\hat{\rho}$ is bounded. Consequently, $\hat{\Upsilon}_0$ is also bounded. Additionally, since $\hat{\Upsilon}_1 > \epsilon$ for $k = 1, 3, 5, \ldots$, the control signal Ω is bounded as well. This implies that $\tilde{\Upsilon}_0$ and $\tilde{\Upsilon}_1$ can be bounded by class $\mathscr{K}$ functions of $\tilde{\sigma}^2$.

Applying now the same reasoning as in the previous proof, we can conclude from (18) that the generator $L(V)$ for $V(\rho) \geq \eta_1(\tilde{\sigma}^2)$ satisfies

$$L(V) \leq -\eta(V) + \eta_0,$$

for some class $\mathscr{K}$ function η, a positive definite function η_1, and a constant $\eta_0 \geq 0$. Therefore, by invoking the results from [17], the desired conclusions follow. □

V. APPLICATION TO QUBITS IN LEAKY CAVITIES

The methodology presented here for the illustrated example is applicable to any two-level atom experiencing classical influences such as driving, damping, and detuning. Our examination specifically focuses on a qubit interacting with a leaky cavity in a rotating frame. The drift Hamiltonian, $H_d = \frac{\omega_R}{2}\sigma_3$, incorporates the effective detuning, $\omega_\Delta = \omega_R + \Delta\omega_R - \omega_0$, which represents the adjusted frequency discrepancy of the qubit. Here, ω_R denotes the frequency gap between the excited $|e\rangle$ and ground $|g\rangle$ states, ω_0 signifies the oscillation frequency of the driving field, and $\Delta\omega_R$ refers to the frequency shift. The Pauli operator $\sigma_3 = |g\rangle\langle g| - |e\rangle\langle e|$ serves as the inversion operator for the qubit. The control Hamiltonian, $H_C = -\Omega(t)\sigma_1$, where $\Omega(t)$ is the Rabi frequency, is directly proportional to the transition dipole moment and the amplitude of the driving electromagnetic field. For the annihilation and creation field operators, we utilize the Pauli lowering and raising operators, $a = \sigma_-$ and $a^\dagger = \sigma_+$, respectively. The initial density operator is chosen as $\rho_0 = \begin{bmatrix} 0.5 & -0.5i \\ 0.5i & 0.5 \end{bmatrix}$ corresponding to the Bloch vector $\mathbf{x}_0 = [0, 1, 0]^T$. The parameters used in simulations are defined as follows: The decay rate (Γ) is set to 10 s^{-1}, representing the rate at which the system loses energy to its environment. The Rabi frequency (ω_R) is 5Γ rad/s, characterizing the frequency of oscillation for a two-level system driven by a resonant electromagnetic field. The interaction strength (M) used in the Lindblad term is set to $1\,s^{-1}$, representing the strength of certain dissipative processes. The detection efficiency (η) is set to 0.8, indicating that 80% of the signals are correctly detected. The time step for numerical integration (dt) is set to 0.001 seconds to improve accuracy, and the total simulation time (T) is set to 1.0 second, defining the duration over which the simulation is run. For now, we consider the amplitude of the driving field (Ω), which represents the strength of the external field, as 3Γ rad/s. We later change this value with the one obtained from control method.

Figure 2 shows our analysis of three distinct scenarios. The first scenario depicts the evolution without dissipation or noise, highlighting the ideal oscillatory behavior resulting from the coherent superposition of quantum states. The second scenario illustrates the dissipative dynamics governed by the Lindblad Equation, modeling how environmental impacts cause the decay of these oscillations. The third scenario introduces stochastic dynamics, where random environmental disturbances are represented by stochastic noise. In this scenario, the stochastic evolution is shown across 100 realizations, with the mean values highlighted to provide a clear understanding of the system's overall behavior.

Figure 3 illustrates a comparative analysis of the quantum filter estimator and the quantum extended Kalman filter estimator for the elements of the coherence vectors. Both filters are initialized with $\hat{\mathbf{x}}_0 = [1, 0, 0]^T$, corresponding to the density matrix $\hat{\rho}_0 = \begin{bmatrix} 0.5 & 0.5 \\ 0.5 & 0.5 \end{bmatrix}$. The analysis reveals that both filters closely track the true state across all three variables, with minor deviations primarily during the initial transient phase. The Kalman filter estimates (red dashed lines) demonstrate faster convergence to the true state compared to the quantum filter estimates (green dashed lines), particularly noticeable in the initial peaks. Despite these differences in the transient phase, both filters achieve nearly identical accuracy in steady-state estimation. The slight deviations observed

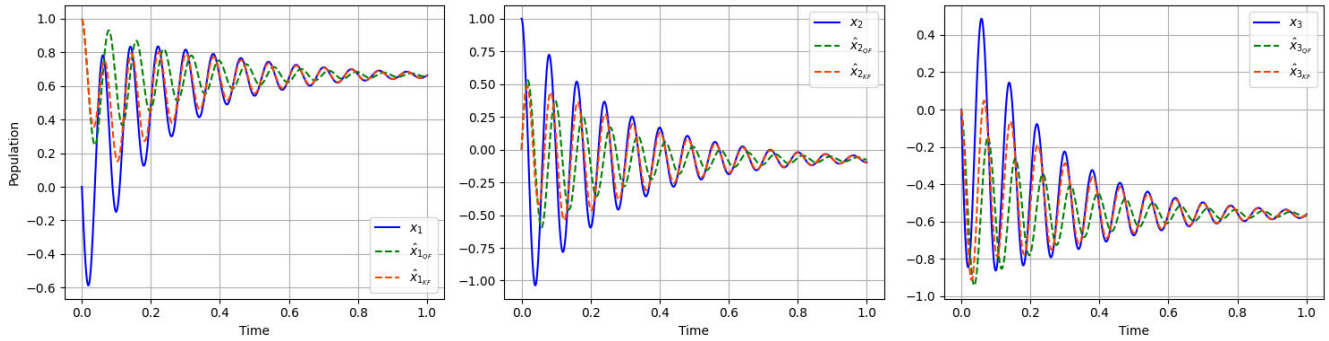

FIGURE 3. Comparative analysis of true state, quantum filter, and quantum extended Kalman filter in the x-representation. The plots show the population dynamics over time for three different state variables in the coherence vector representation: (a) x_1, (b) x_2, and (c) x_3. The blue solid lines represent the true state (x_1, x_2, x_3), the green dashed lines represent the estimates obtained from the quantum filter ($\hat{x}_{1QF}, \hat{x}_{2QF}, \hat{x}_{3QF}$), and the red dashed lines represent the estimates from the Kalman filter ($\hat{x}_{1KF}, \hat{x}_{2KF}, \hat{x}_{3KF}$).

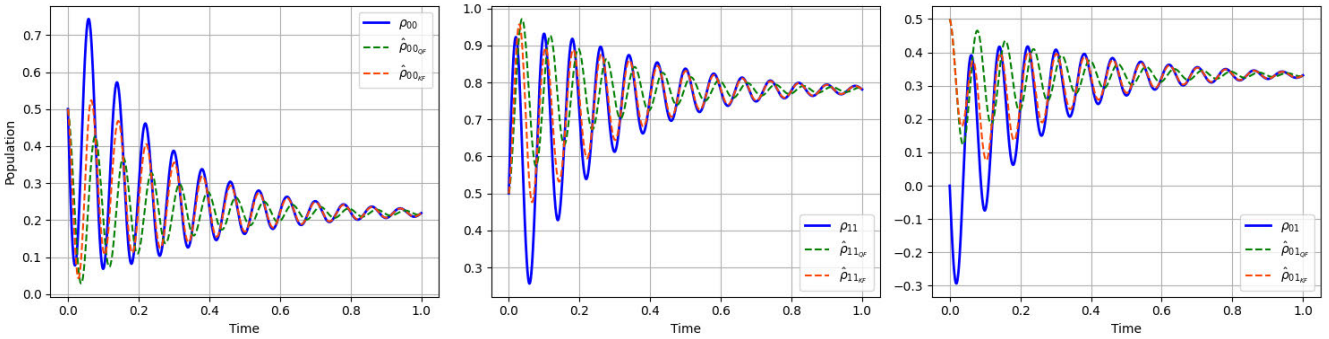

FIGURE 4. Comparison of true density matrix elements with quantum and quantum extended Kalman filter estimates. The plots display the evolution of the real parts of the density matrix elements over time, comparing the true values (solid blue lines) with the estimates obtained from the quantum filter (dashed green lines) and the Kalman filter (dashed red lines).

in the quantum filter during the early phase indicate a higher sensitivity to initial conditions and noise, which gradually corrects over time. Overall, both filters effectively estimate the quantum state's dynamics, offering valuable insights into the system's behavior.

Figure 4 shows the reconstruction of the density matrix $\hat{\rho}(t)$ from the elements of the coherence vector $\hat{\mathbf{x}}$. This process involves transforming the state space representation back into the density matrix form, ensuring that the estimates are consistent with the physical properties of the quantum state. The figure demonstrates that both the quantum filter and the quantum extended Kalman filter estimates converge to the true values for all elements. Notably, the Kalman filter exhibits faster convergence. In the steady-state region, both filters provide estimates that closely match the true values, indicating their robustness for long-term state estimation. Although minor discrepancies are observed during the transient phase, these are corrected over time, with both filters showing high fidelity in tracking the true state of the system. This analysis highlights the robustness and accuracy of both the quantum and Kalman filters in estimating the state of a quantum system.

Figure 5 shows the fidelity between the true density operator and the estimated state, computed using

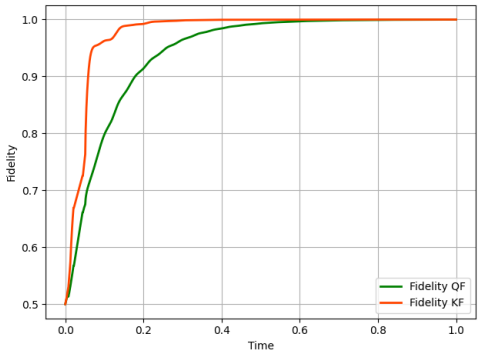

FIGURE 5. Fidelity comparison over time between true and estimated density matrices. The plot shows the fidelity values between the true density matrix and the estimates obtained from the Kalman filter and the quantum filter over time.

$F(\rho, \hat{\rho}) = \left(\mathrm{Tr}\left(\sqrt{\sqrt{\rho}\hat{\rho}\sqrt{\rho}}\right)\right)^2$ for both the quantum filter and Kalman filter. This measure quantifies the proximity of the estimated density matrix to the true density matrix, with values ranging from 0 (completely different) to 1 (identical). The figure illustrates that both filters achieve high fidelity with the true state, particularly in the steady state, indicating accurate tracking of the quantum state. While there are slight

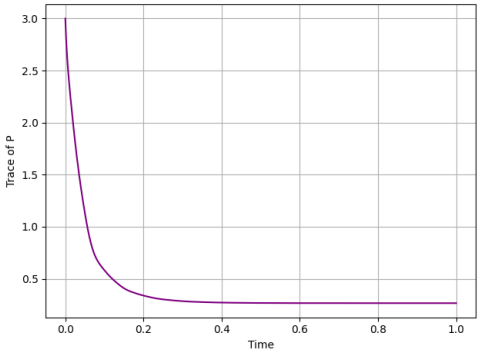

FIGURE 6. Evolution of the Trace of the Error Covariance Matrix P over Time. The plot shows the trace of the error covariance matrix P as a function of time in the Kalman filtering process. The trace of P is a scalar measure of the total estimation error variance across all state variables.

discrepancies initially, both filters converge to high fidelity values, demonstrating their effectiveness in quantum state estimation. The transient region displays fluctuations, reflecting the filters' adaptation to the initial state dynamics. The Kalman filter exhibits slightly faster convergence compared to the quantum filter, which is particularly important for real-time applications. It is important to emphasize that the Kalman filter offers the significant advantage of allowing the tuning of its gains (specifically, the covariances Q and R) to enhance performance. In contrast, the Quantum filter lacks this flexibility.

Figure 6 delves deeper into the analysis of the proposed Kalman filtering by showing the trace of the error covariance matrix P. The trace of P can be seen (in an ideal scenario) as an indicator of the Kalman filter's performance, as it quantifies the evolution of uncertainty in the state estimates, demonstrating the filter's effectiveness in reducing this uncertainty over time. As depicted in the figure, the trace of P is initially high, reflecting significant uncertainty in the initial state estimates, which is typical at the start of the filtering process when the initial state is often based on a rough estimate. As the Kalman filter processes measurements, the trace of P decreases, indicating that the filter effectively reduces uncertainty in the state estimates by incorporating new measurement information. This reduction is evident from the rapid decline in the trace of P during the initial phase of filtering. Eventually, the trace of P reaches a steady-state value, signifying that the filter has minimized the uncertainty in the state estimates. The steady-state value of the trace of P is influenced by process noise and measurement noise.

Figure 7 shows the time evolution of the quantum state populations x_1, x_2, and x_3 under multiple model implementations for both quantum and Kalman filtering approaches. Each row corresponds to a specific ω_R multiplier (0.8, 0.9, 1.0, 1.1, 1.2), and each column represents a state variable. When ω_R is set to the nominal value (1.0), both QF and KF estimates converge to the true states, demonstrating accuracy and robustness. However, for other ω_R values, discrepancies between the true states and filter estimates become noticeable, highlighting the system's sensitivity to variations in ω_R. These results underscore the robustness of the MMAE approach, where dynamic weights adjust

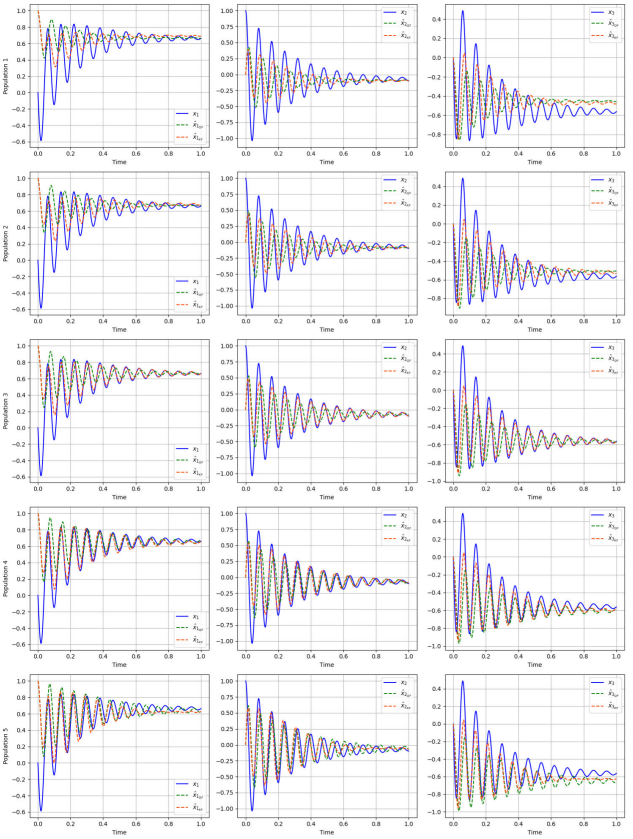

FIGURE 7. Time Evolution of quantum state populations with multiple models of ω_R. This figure illustrates the dynamic behavior of the quantum state populations x_1, x_2, and x_3 under varying ω_R values, with true states shown in blue, quantum filter estimates in green, and Kalman filter estimates in orange. Each row corresponds to a different ω_R multiplier: 0.8 (Population 1), 0.9 (Population 2), 1 (Population 3), 1.1 (Population 4), and 1.2 (Population 5). Columns represent the state variables x_1, x_2, and x_3 respectively. The plots highlight the performance of the QF and KF in tracking the true quantum state across different ω_R scenarios.

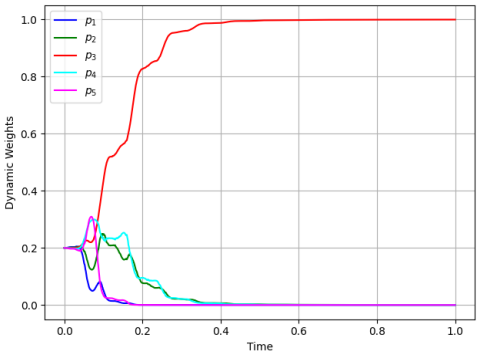

FIGURE 8. Dynamic evolution of model weights p_i in the MMAE framework. This figure illustrates the time evolution of the dynamic weights p_1, p_2, p_3, p_4, and p_5 associated with different models in the MMAE. The weights are represented to show their adaptation over time as the MMAE converges to the most probable model.

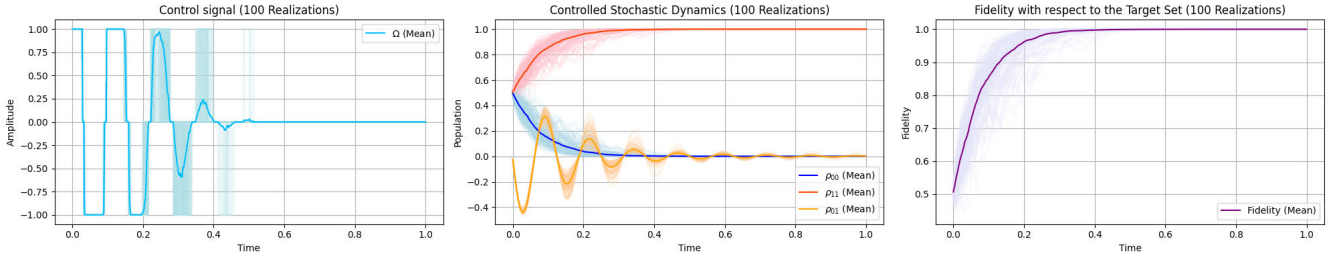

FIGURE 9. Control signal, controlled state evolution, and fidelity over 100 stochastic realizations. The first subplot displays the control signal $\Omega(t)$ applied over time for 100 realizations (light blue lines) with the mean control signal. The second subplot illustrates the controlled time evolution of the elements of the density operator, depicting how the state evolves towards the target set. The third subplot presents the fidelity with respect to the target state, demonstrating that the target state is achieved with high accuracy.

the contributions of each model based on the observed data. The adaptive nature of the MMAE ensures that the most probable model predominantly influences the state estimation, effectively handling uncertainties in ω_R. This adaptability is crucial for maintaining accurate state estimates in quantum systems with variable dynamics, providing a reliable framework for practical quantum state monitoring and control applications.

Figure 8 demonstrates the dynamic adaptation of model weights in the MMAE framework. Each weight p_i corresponds to a model with a different ω_R multiplier. Initially, all weights are set equally, reflecting no prior knowledge about which model is most accurate. As the estimation process progresses, the weights dynamically adjust based on the error measures between the observed measurements and the predicted states from each model. This adjustment is governed by a dynamic recursion equation, enabling the MMAE to identify and emphasize the most likely model over time. The results show that the weight p_3, corresponding to the nominal ω_R, gradually becomes dominant as the most probable model. This is evidenced by its increase and stabilization at a higher value compared to the other weights, which decrease as the system identifies them as less probable. The convergence of p_3 demonstrates the effectiveness of the MMAE in correctly identifying the model that best represents the true system dynamics. The variations and eventual stabilization of the weights illustrate the MMAE's capability to adapt to the true system parameters, ensuring robust state estimation even under model uncertainties. This dynamic adaptation is crucial for accurately tracking the quantum state in systems where parameters may not be precisely known or may vary over time.

Figure 9 presents our results regarding the dynamic control of the studied quantum system under stochastic influences, with the goal of steering the system towards a specified target set. All simulations are conducted over 100 realizations to account for the effects of noise and randomness. The first subplot displays the control signal $\Omega(t)$ over time for each of the 100 realizations, shown in light blue, with the mean control signal highlighted. This control signal is dynamically adjusted using feedback from the system's state to steer the system towards the desired target state, employing our Lyapunov switching approach. The variability in the control signals across realizations reflects the system's adaptive response to stochastic disturbances. The second subplot shows the evolution of the density matrix elements over time, with the control signal $\Omega(t)$ used to achieve controlled evolution. This plot illustrates the convergence of the state populations' trajectory towards the desired target under the applied control signal. The third subplot focuses on the fidelity of the system's state relative to the target, computed as $F(\rho, \rho_f) = \left(\mathrm{Tr}\left(\sqrt{\sqrt{\rho_f}\rho\sqrt{\rho_f}}\right)\right)^2$ for $\rho_f \in \chi_f$. This plot confirms that the control strategy effectively drives the system towards the target state, as evidenced by the high fidelity values over time.

VI. CONCLUSION

We presented a robust framework for controlling stochastic dynamics in quantum systems, particularly focusing on qubits under homodyne detection. The key contributions can be summarized as follows:

We compared traditional quantum filtering with an extended Kalman filtering approach. The Kalman filter demonstrated superior performance due to its tunable covariances, allowing for faster convergence of estimation errors while effectively managing correlated noise.

To address uncertainties in quantum-mechanical Hamiltonians and other system parameters, we introduced a multiple model estimation scheme. This approach significantly improved estimation accuracy under varying conditions.

The estimated state variables from our filtering methods were utilized in a switching-based Lyapunov control scheme, achieving noise-to-state practical stability. This approach successfully stabilized a qubit in a leaky cavity even in the presence of resonance frequency uncertainties.

The techniques developed in this paper have significant potential applications in quantum information processing and metrology. Future research will focus on extending these methods to more complex quantum systems and real-time implementations. An alternative approach to state estimation treats the disturbances as unknown deterministic signals and seeks to optimize some measure of size or "badness" of these signals. The most prominent techniques in the latter domain are H_∞-filtering and minimum-energy

filtering, [23]. Additionally, improvements in quantum state estimation, particularly in handling uncertainties and achieving greater accuracy, are crucial. Exploring cross-disciplinary approaches, such as those discussed in [24] and [25], may further enhance the robustness of quantum control systems.

ACKNOWLEDGMENT

The work has been done in honor and memory of Prof. Fernando Lobo Pereira.

REFERENCES

[1] C. Sayrin, I. Dotsenko, X. Zhou, B. Peaudecerf, T. Rybarczyk, S. Gleyzes, P. Rouchon, M. Mirrahimi, H. Amini, M. Brune, J.-M. Raimond, and S. Haroche, "Real-time quantum feedback prepares and stabilizes photon number states," *Nature*, vol. 477, no. 7362, pp. 73–77, Sep. 2011.
[2] V. Belavkin, "Theory of the control of observable quantum systems," *Automatica Remote Control*, vol. 44, no. 2, pp. 178–188, 1983.
[3] V. P. Belavkin, "Quantum stochastic calculus and quantum nonlinear filtering," *J. Multivariate Anal.*, vol. 42, no. 2, pp. 171–201, Aug. 1992.
[4] L. Bouten, R. Van Handel, and M. R. James, "An introduction to quantum filtering," *SIAM J. Control Optim.*, vol. 46, no. 6, pp. 2199–2241, Jan. 2007.
[5] J. E. Gough, M. R. James, H. I. Nurdin, and J. Combes, "Quantum filtering for systems driven by fields in single-photon states or superposition of coherent states," *Phys. Rev. A, Gen. Phys.*, vol. 86, no. 4, Oct. 2012, Art. no. 043819.
[6] P. Rouchon and J. F. Ralph, "Efficient quantum filtering for quantum feedback control," *Phys. Rev. A, Gen. Phys.*, vol. 91, no. 1, Jan. 2015, Art. no. 012118.
[7] M. F. Emzir, M. J. Woolley, and I. R. Petersen, "A quantum extended Kalman filter," *J. Phys. A, Math. Theor.*, vol. 50, no. 22, 2017, Art. no. 225301.
[8] M. Mirrahimi and R. Van Handel, "Stabilizing feedback controls for quantum systems," *SIAM J. Control Optim.*, vol. 46, no. 2, pp. 445–467, Jan. 2007.
[9] S. C. Hou, M. A. Khan, X. X. Yi, D. Dong, and I. R. Petersen, "Optimal Lyapunov-based quantum control for quantum systems," *Phys. Rev. A, Gen. Phys.*, vol. 86, no. 2, Aug. 2012, Art. no. 022321.
[10] G. Cardona, A. Sarlette, and P. Rouchon, "Exponential stochastic stabilization of a two-level quantum system via strict Lyapunov control," in *Proc. IEEE Conf. Decis. Control (CDC)*, Dec. 2018, pp. 6591–6596.
[11] T. Grigoletto and F. Ticozzi, "Stabilization via feedback switching for quantum stochastic dynamics," *IEEE Control Syst. Lett.*, vol. 6, pp. 235–240, 2022.
[12] W. Liang, T. Grigoletto, and F. Ticozzi, "Dissipative feedback switching for quantum stabilization," *Automatica*, vol. 165, Jul. 2024, Art. no. 111659.
[13] K. Ma, J. Kong, Y. Wang, and X.-M. Lu, "Review of the applications of Kalman filtering in quantum systems," *Symmetry*, vol. 14, no. 12, p. 2478, Nov. 2022.
[14] E. Corcione and C. Tarin, "State and parameter estimation for stochastic open two-level quantum systems," in *Proc. Amer. Control Conf. (ACC)*, May 2023, pp. 2270–2275.
[15] P. Rouchon, "A tutorial introduction to quantum stochastic master equations based on the qubit/photon system," *Annu. Rev. Control*, vol. 54, pp. 252–261, Mar. 2022.
[16] H. Ito and Y. Nishimura, "Stability of stochastic nonlinear systems in cascade with not necessarily unbounded decay rates," *Automatica*, vol. 62, pp. 51–64, Dec. 2015.
[17] H. Deng, M. Krstic, and R. J. Williams, "Stabilization of stochastic nonlinear systems driven by noise of unknown covariance," *IEEE Trans. Autom. Control*, vol. 46, no. 8, pp. 1237–1253, Aug. 2001.
[18] D. Simon, *Optimal State Estimation: Kalman, H Infinity, and Nonlinear Approaches*. Hoboken, NJ, USA: Wiley, 2006.
[19] R. Alicki and K. Lendi, "N-level systems and applications to spectroscopy," in *Quantum Dynamical Semigroups and Applications* (Lecture Notes in Physics), vol. 717. Berlin, Germany: Springer, 2007, pp. 47–107.
[20] V. Hassani, A. P. Aguiar, M. Athans, and A. M. Pascoal, "Multiple model adaptive estimation and model identification usign a minimum energy criterion," in *Proc. Amer. Control Conf.*, Jun. 2009, pp. 518–523.
[21] D. d'Alessandro, *Introduction to Quantum Control and Dynamics*. Boca Raton, FL, USA: CRC Press, 2021.
[22] A. Pedro Aguiar, J. P. Hespanha, and A. M. Pascoal, "Switched seesaw control for the stabilization of underactuated vehicles," *Automatica*, vol. 43, no. 12, pp. 1997–2008, Dec. 2007.
[23] A. Saccon, J. Trumpf, R. Mahony, and A. P. Aguiar, "Second-order-optimal minimum-energy filters on lie groups," *IEEE Trans. Autom. Control*, vol. 61, no. 10, pp. 2906–2919, Oct. 2016.
[24] Y. Wang, Y. Xia, P. Zhou, and D. Duan, "A new result on H-infinity state estimation of delayed static neural networks," *IEEE Trans. Neural Netw. Learn. Syst.*, vol. 28, no. 12, pp. 3096–3101, Dec. 2016.
[25] A. Loquercio, M. Segu, and D. Scaramuzza, "A general framework for uncertainty estimation in deep learning," *IEEE Robot. Autom. Lett.*, vol. 5, no. 2, pp. 3153–3160, Apr. 2020.

NAHID BINANDEH DEHAGHANI (Graduate Student Member, IEEE) is currently pursuing the Ph.D. degree in electrical and computer engineering with the Faculty of Engineering, University of Porto, Portugal. Since 2019, she has been a Researcher with the SYSTEC-ARISE Research Center for Systems and Technologies. Her research interests include the control and optimization of quantum systems, quantum computing, and quantum information processing.

A. PEDRO AGUIAR (Senior Member, IEEE) received the Ph.D. degree in electrical and computer engineering from IST, University of Lisbon, in 2002. He is currently a Full Professor with the Faculty of Engineering, University of Porto (FEUP). He is also the Director of the Advanced Production and Intelligent Systems Associate Laboratory (ARISE) and a Scientific Coordinator of the Research Center for Systems and Technologies (SYSTEC). His academic journey includes post-doctoral research at the University of California at Santa Barbara (UCSB), from 2002 to 2005, and teaching positions at FEUP and IST. His research interests include control systems (theory and applications), including motion planning, autonomous robotic vehicles, nonlinear control theory, integration of machine learning with feedback control, quantum feedback systems, and large-scale distributed systems.

RAFAL WISNIEWSKI (Senior Member, IEEE) received the Ph.D. degree in electrical engineering and the Ph.D. degree in mathematics from Aalborg University, Aalborg, Denmark, in 1997 and 2005, respectively. From 2007 to 2008, he was a Control Specialist with Danfoss A/S. Currently, he is a Professor and the Head of the Learning and Decision Laboratory and the Deputy Head for Research with the Department of Electronic Systems, Aalborg University. His research interests include system theory, safety, security, and quantum control.